Electronic Supplementary Material (ESI) for CrystEngComm.

Anion-templated 2D frameworks from hexahydroxytriphenylene

Mahbod Morshedi, Anthony C. Willis and Nicholas G. White*

Research School of Chemistry, Australian National University
137 Sullivan's Creek Road, Acton, 2601, ACT, Australia
Email: nicholas.white@anu.edu.au
URL: www.nwhitegroup.com

Experimental considerations and details of instrumentation

Dry dichloromethane was prepared by distillation from CaH_2. All other chemicals were purchased from commercial suppliers and used as received.

NMR spectra were collected on Varian Gemini or Bruker Avance 400 spectrometers and are referenced to the residual solvent signal.[S1] Infrared spectra were recorded on a Perkin-Elmer Spectrum Two FT-IR Spectrometer fitted with a UATR Two Single Reflection Diamond. Thermogravimetric analysis traces were recorded in an oxygen atmosphere using a TA Instruments Q500 analyser.

Details of instruments used to record PXRD and SCXRD data are given in the respective sections of the Supporting Information.

Synthesis and characterisation

Synthesis of HHTP

HHTP has been prepared directly from catechol using ammonium persulfate as oxidant,[S2] however we were unable to reproduce this synthesis. A hypervalent iodine reagent in acidic media has also been reported to affect this direct cyclooxidation but this uses expensive hexafluoroisopropanol as solvent.[S3] We found that oxidative trimerisation of 1,2-dimethoxybenzene using $FeCl_3$ in CH_2Cl_2 smoothly gave hexamethoxytriphenylene (**HMTP**), which could be isolated in reasonable yield by simply adding methanol to the crude reaction to precipitate clean **HMTP**.[S4] We did not attempt to optimise this procedure, so higher yields may well be achievable.

Deprotection of **HMTP** using $HBr_{(aq)}$ and HOAc, resulted in crude **HHTP** with a deep purple colour (presumably due to quinoid impurities[S5]) that was difficult to purify (difficulties purifying **HHTP** have been previously reported[S5]). Instead we used BBr_3 in CH_2Cl_2 to deprotect **HMTP**[S6] giving essentially pure **HHTP**. Clean product was obtained in reasonable yield by precipitating **HHTP** from methanol with water.

2,3,6,7,10,11-Hexamethoxytriphenylene, HMTP

Anhydrous $FeCl_3$ (14.6 g, 90.0 mmol) was added to CH_2Cl_2 (100 mL) and the mixture was stirred at room temperature under a nitrogen atmosphere and veratrole (3.82 mL, 4.15 g, 30.0 mmol) was added dropwise. Stirring at room temperature under a nitrogen atmosphere was continued for 90 minutes, after which time the reaction was poured into methanol (200 mL), causing immediate precipitation of a pale product. The mixture was left to stand in a freezer overnight, the solid was isolated by filtration and washed with ethanol (2 × 10 mL), then methanol (3 × 10 mL) and dried *in vacuo* to give **HMTP** as a pale grey powder. Yield: 1.90 g (4.65 mmol, 47%).
^{1}H NMR ($CDCl_3$): 7.76 (s, 6H), 4.12 (s, 18H) ppm. ^{13}C NMR ($CDCl_3$): 148.9, 123.3, 104.4, 56.2 ppm.

2,3,6,7,10,11-Hexahydroxytriphenylene, HHTP

HMTP (0.200 g, 0.490 mmol) was suspended in dry dichloromethane (10 mL), and the mixture was cooled to 0 °C under a nitrogen atmosphere, and a solution of boron tribromide in dichloromethane (1.0 M, 3.5 mL, 3.5 mmol) was added. The reaction mixture was stirred for 6 hours, poured into ice water (100 mL) and stirred for 30 minutes. The resulting purple precipitate was isolated by filtration, dissolved in methanol (5 mL), and re-precipitated by addition of water (100 mL). The precipitate was isolated by filtration, washed with diethyl ether (2 × 10 mL) and dried *in vacuo* to give **HHTP** as a pale blue powder. Yield: 0.88 g (56%).
^{1}H NMR (d_6-DMSO): 9.29 (br. s, 6H), 7.60 (s, 6H) ppm. ^{13}C NMR (d_6-acetone): 145.9, 123.9, 108.7ppm.

Synthesis of anion-templated framework materials

General procedure: A mixture of **HHTP** (20 mg, 0.062 mmol) and one molar equivalent of tetraalkylammonium salt were dissolved in methanol (6 mL). These solutions were subjected to diethyl ether vapour diffusion, which gave the products as pale brown crystals. These were isolated by filtration, washed with copious diethyl ether, and air-dried (subsequent NMR analysis showed that there was no methanol/diethyl ether solvent remaining within the crystals after this drying process, see Figs. S3–S10). Structures were determined by SCXRD, and PXRD used to show that the structure of the bulk material was consistent with that determined by SCXRD.

$[HHTP{\cdot}TBA{\cdot}Cl]_n$

Yield: 28 mg (75%). ^{1}H NMR (d_6-DMSO): 9.32 (br. s, 6H), 7.61 (s, 6H), 3.10–3.20 (m, 8H), 1.49–1.62 (m, 8H), 1.24–1.36 (m, 8H), 0.93 (t, J = 7.1 Hz, 12H) ppm. IR (*inter alia*): 3459 (O–H stretch), 3177 (O–H stretch), 1626 (C–C stretch), 1598 (C–C stretch) cm^{-1}.

[HHTP·TBA·I]$_n$

Yield: 30 mg (70%). ^{1}H NMR (d_6-DMSO): 9.30 (br. s, 6H), 7.60 (s, 6H), 3.11–3.20 (m, 8H), 1.50–1.62 (m, 8H), 1.24–1.37 (m, 8H), 0.93 (t, *J* = 7.2 Hz, 12H) ppm. IR (*inter alia*): 3410 (O–H stretch), 3204 (O–H stretch), 1631 (C–C stretch), 1600 (C–C stretch) cm^{-1}.

[HHTP·TBA·H_2PO_4]$_n$

Yield: 34 mg (83%). ^{1}H NMR (d_6-DMSO): 7.65 (s, 6H), 3.10–3.18 (m, 8H), 1.47–1.61 (m, 8H), 1.23–1.35 (m, 8H), 0.92 (t, *J* = 7.2 Hz, 12H) ppm . IR (*inter alia*): 3520 (O–H stretch), 3266 (O–H stretch), 1631 (C–C stretch), 1621 (C–C stretch), 1603 (C–C stretch) cm^{-1}.

[HHTP·TBA·OAc]$_n$

Yield: 26 mg (67%). ^{1}H NMR (d_6-DMSO): 7.57 (s, 6H), 3.08–3.19 (m, 8H), 1.73 (s, 3H), 1.49–1.61 (m, 8H), 1.23–1.35 (m, 8H), 0.92 (t, *J* = 7.2 Hz, 12H) ppm . IR (*inter alia*): 3535 (O–H stretch), 3339 (O–H stretch), 1611 (C–C stretch) cm^{-1}.

[HHTP·TBA·0.5HSO_4·0.5$MeOSO_3$]$_n$

Yield: 17 mg (41%). ^{1}H NMR (d_6-DMSO): 7.59 (s, 6H), 3.09–3.20 (m), 1.49–1.61 (m, 8H), 1.24–1.36 (m, 8H), 0.93 (t, *J* = 7.2 Hz, 12H) ppm. IR (*inter alia*): 3349 (O–H stretch), 3171 (O–H stretch), 1619 (C–C stretch), 1603 (C–C stretch) cm^{-1}.

Note: an additional resonance appears to be present, which we assign to the methylsulfate group, but this peak overlaps with the water resonance in d_6-DMSO. NMR analysis in CD_3OD suggests approximately 50% of the anion is present as $MeOSO_3^-$, see p.7 of Supporting Information and Figs. S7, S9 and S10.

[HHTP·TEA·Cl]$_n$

Yield: 25 mg (83%). ^{1}H NMR (d_6-DMSO): 9.31 (br. s, 6H), 7.60 (s, 6H), 3.19 (q, *J* = 7.2 Hz, 8H), 1.15 (t, *J* = 7.2 Hz, 12H). IR (*inter alia*): 3434 (O–H stretch), 3160 (O–H stretch), 1632 (C–C stretch), 1600 (C–C stretch) cm^{-1}.

^{1}H NMR spectra of HMTP, HHTP and anion-templated framework materials

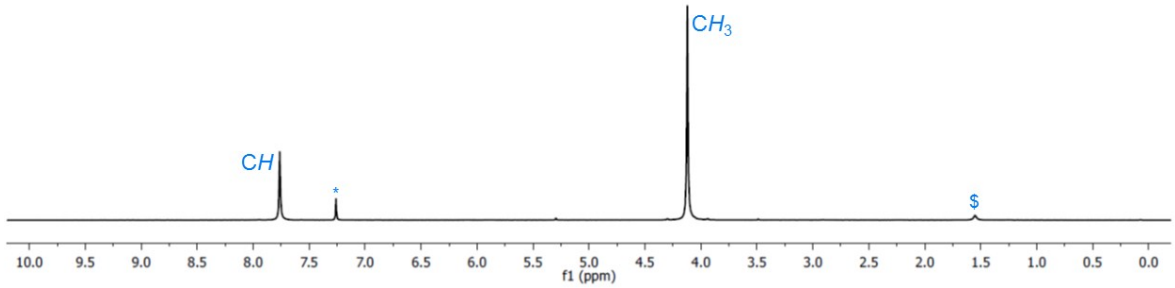

Fig. S1 ^{1}H NMR spectrum of **HMTP** ($CDCl_3$, 298 K; peak marked * corresponds to residual solvent peak, peak marked $ corresponds to water).

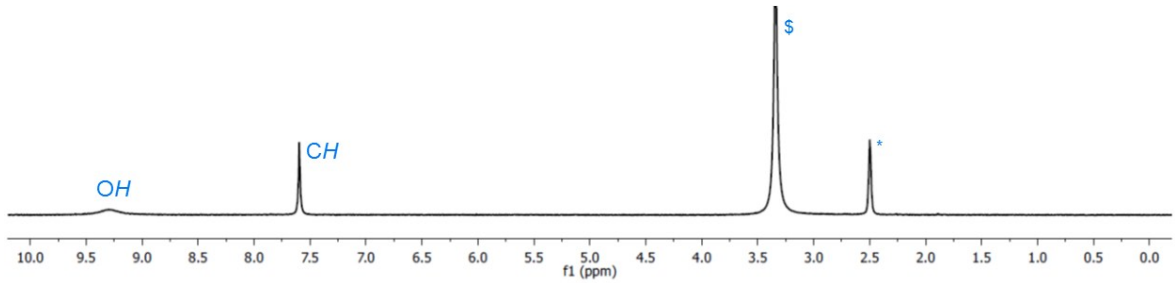

Fig. S2 ^{1}H NMR spectrum of **HHTP** (d_6-DMSO, 298 K; peak marked * corresponds to residual solvent peak, peak marked $ corresponds to water).

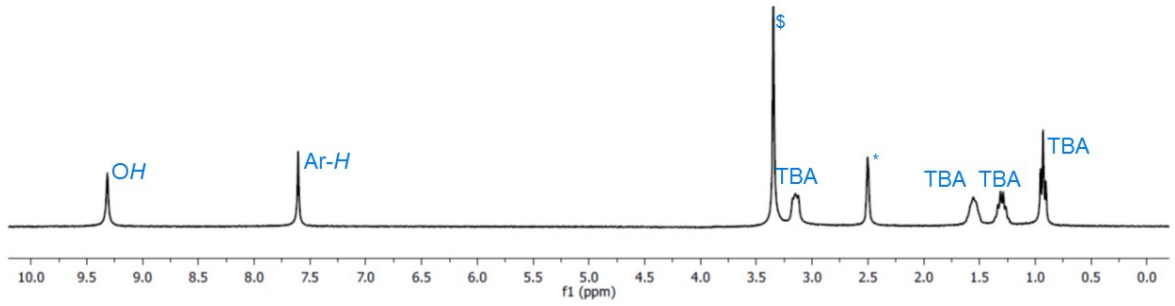

Fig. S3 ^{1}H NMR spectrum of [**HHTP**·TBA·Cl]$_n$ (d_6-DMSO, 298 K; peak marked * corresponds to residual solvent peak, peak marked $ corresponds to water).

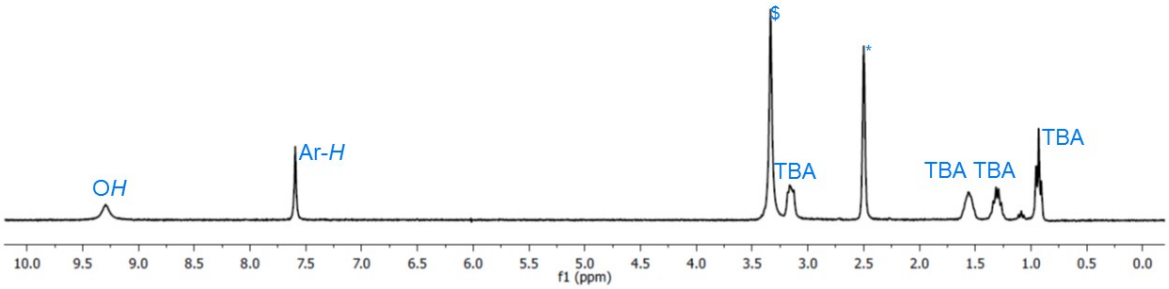

Fig. S4 ^{1}H NMR spectrum of [**HHTP**·TBA·I]$_n$ (d_6-DMSO, 298 K; peak marked * corresponds to residual solvent peak, peak marked $ corresponds to water).

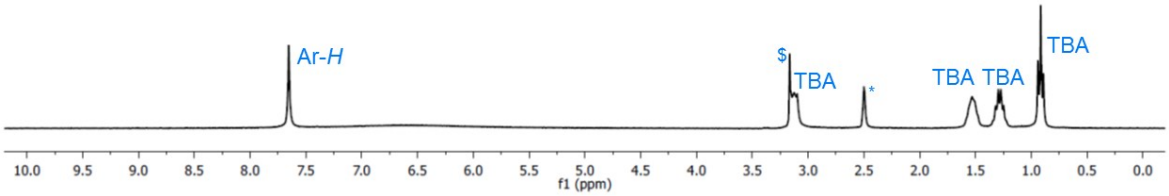

Fig. S5 ^{1}H NMR spectrum of [**HHTP**·TBA·H_2PO_4]$_n$ (d_6-DMSO, 298 K; peak marked * corresponds to residual solvent peak, peak marked $ corresponds to water).

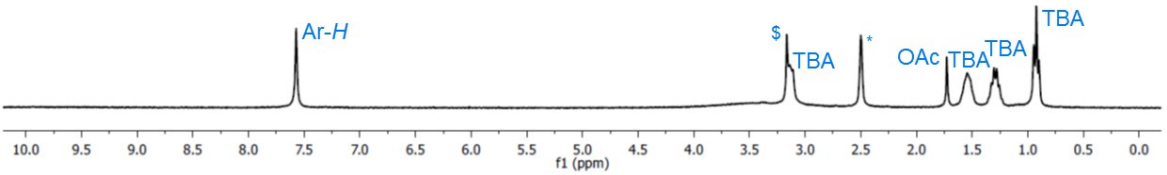

Fig. S6 ^{1}H NMR spectrum of [**HHTP**·TBA·OAc]$_n$ (d_6-DMSO, 298 K; peak marked * corresponds to residual solvent peak, peak marked $ corresponds to water).

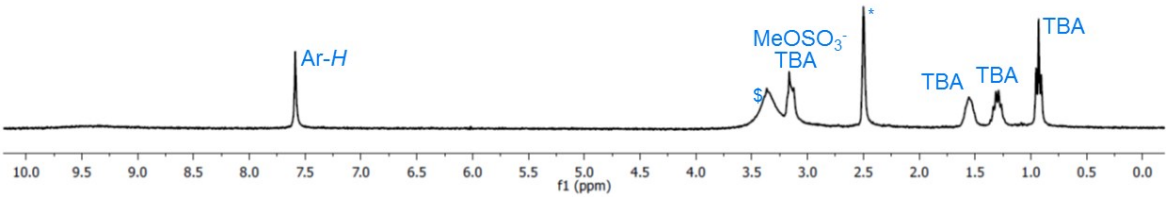

Fig. S7 ^{1}H NMR spectrum of [**HHTP**·TBA·0.5HSO_4·0.5$MeOSO_3$]$_n$ (d_6-DMSO, 298 K; peak marked * corresponds to residual solvent peak, peak marked $ corresponds to water).

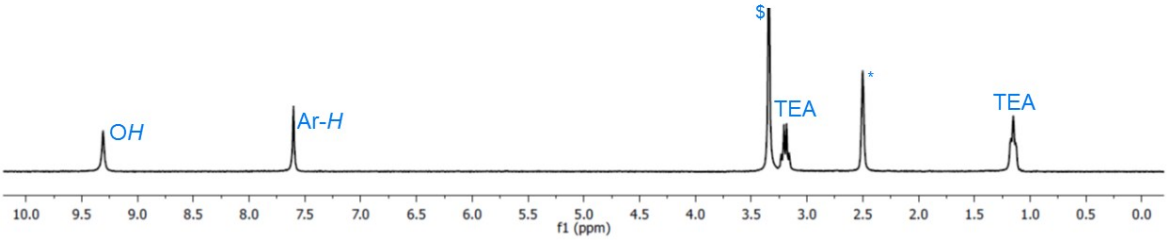

Fig. S8 ^{1}H NMR spectrum of [**HHTP**·TEA·Cl]$_n$ (d_6-DMSO, 298 K; peak marked * corresponds to residual solvent peak, peak marked $ corresponds to water).

Additional NMR spectra of [HHTP·TBA·0.5HSO$_4$·0.5MeOSO$_3$]$_n$

As the methylsulfate peak of [**HHTP**·TBA·0.5HSO$_4$·0.5MeOSO$_3$]$_n$ overlaps with other resonances in the ^{1}H NMR spectrum in d$_6$-DMSO, we collected a spectrum in CD$_3$OD to allow quantification of the conversion of HSO$_4^-$ to MeOSO$_3^-$ (Fig. S9). This suggested approximately half conversion (*i.e.* half of the anion present as MeOSO$_3^-$, with the other half presumably HSO$_4^-$). ^{13}C NMR spectroscopy (Fig. S10) also showed a singlet peak at 55.1 ppm, which we attribute to the MeOSO$_3^-$ anion.

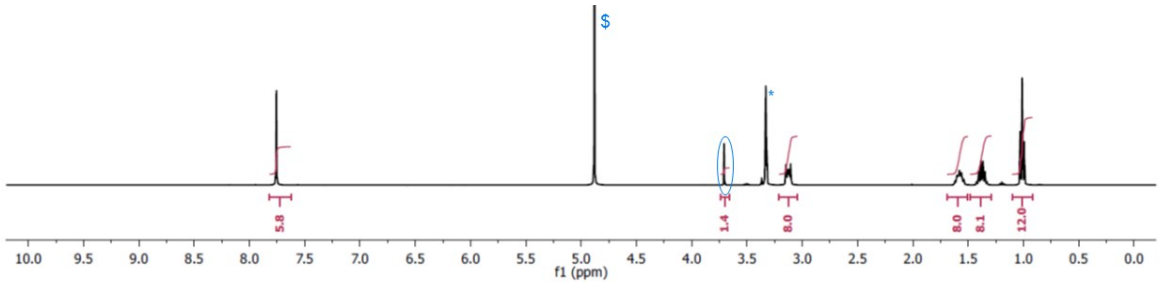

Fig. S9 ^{1}H NMR spectrum of [**HHTP**·TBA·0.5HSO$_4$·0.5MeOSO$_3$]$_n$ showing approximately half conversion of HSO$_4^-$ to MeOSO$_3^-$ (CD$_3$OD, 298 K; peak marked * corresponds to residual solvent peak, peak marked $ corresponds to water, circled peak is attributed to MeOSO$_3^-$ anion).

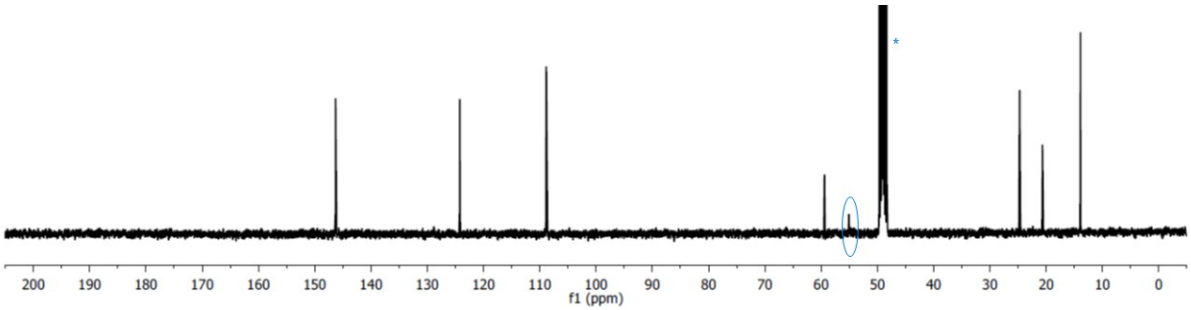

Fig. S10 ^{13}C NMR spectrum of [**HHTP**·TBA·0.5HSO$_4$·0.5MeOSO$_3$]$_n$ (CD$_3$OD, 298 K; peak marked * corresponds to residual solvent peak, circled peak is attributed to MeOSO$_3^-$ anion).

Details of SCXRD experiments and additional figures of solid state structures

General comments

Data were either collected using graphite-monochromated Mo Kα radiation using an Agilent Xcalibur diffractometer, or using mirror-monochromated Cu Kα radiation using an Agilent SuperNova diffractometer. Crystals were cooled to 150 K using a Cryostream N2 open-flow cooling device[S7] in all cases. Raw frame data (including data reduction, interframe scaling, unit cell refinement and absorption corrections) were processed using CrysAlisPro.[S8]

Structures were solved with SUPERFLIP[S9] and refined using full-matrix least-squares of F^2 within the CRYSTALS suite.[S10] All non-hydrogen atoms were refined with anisotropic displacement parameters. C–H hydrogen atoms were generally visible in the Fourier difference map, and were initially refined with restraints on bond lengths and angles, after which the positions were used as the basis for a riding model.[S11] O–H hydrogen atoms were generally visible in the Fourier difference map and were refined with restraints on bond lengths and angles.

A summary of crystallographic details is given in Table S1, full crystallographic data in CIF format are provided as Supporting Information (CCDC Numbers: 1451578–1451583). Individual structures are discussed in more detail below.

Comments on hydrogen bonding parameters

As hydrogen atom positions cannot be determined precisely by conventional X-ray diffraction, these hydrogen bonding parameters are approximate only, and hence are given only to a small number of significant figures. No errors are given for these values as the errors calculated by common crystallographic software for distances involving hydrogen atoms have little or no chemical significance. R–H distances (such as O–H distances) are known to be underestimated by X-ray crystallography,[S12] so in fact H···X distances and %vdW parameters are probably overestimated. That is, the true O–H bond length is probably longer, and the true H···X distance shorter than reported (and therefore the true %vdW parameter is probably lower than reported).

Comments on individual structures

*Co-crystals of **HHTP** with TBA·Cl*

The structure crystallises in the polar space group *P*c with Z′ = 2. One of the two crystallographically-independent TBA cations is positionally disordered and the structure required restraints on the bond lengths and angles, and thermal and vibrational ellipsoid parameters of both TBA cations to achieve a sensible refinement.

*Co-crystals of **HHTP** with TBA·I*

The structure crystallises in the monoclinic space group $P2_1/c$ with Z′ = 2 with one half-occupancy co-crystallised water molecule. The terminal carbon atom of one butyl group of one TBA cation is disordered and the structure required restraints on TBA bond lengths, as well as on the angles of the disordered methyl group to achieve a sensible refinement.

*Co-crystals of **HHTP** with TBA·H_2PO_4*

The structure crystallises in the monoclinic space group $P2_1/n$ with one co-crystallised methanol molecule. The terminal carbon atom of one butyl group of the TBA cation is disordered and the structure required restraints on bond lengths and angles involving this disordered atom.

*Co-crystals of **HHTP** with TBA·OAc*

The structure crystallises in the monoclinic space group $P2_1/n$ with one co-crystallised methanol molecule. The terminal carbon atom of three butyl groups of the TBA cation is disordered and the structure required restraints on the bond lengths and angles, and thermal and vibrational ellipsoid

parameters of both TBA cations to achieve a sensible refinement. A small amount of residual electron density is located around the TBA cation, which could not be sensibly modelled.

*Co-crystals of **HHTP** with TBA·HSO_4*

The structure crystallises in the monoclinic space group $P2_1/c$ with $Z' = 2$. Crystals are twinned, and the ROTAX[S13] programme within CRYSTALS[S10] was used to find and apply a suitable twin law. One of the two crystallographically-independent TBA cations is positionally disordered and the structure required restraints on the bond lengths and angles, and thermal and vibrational ellipsoid parameters of this TBA cation, as well as on the bond lengths and angles, and thermal and vibrational ellipsoid parameters of one of the $MeOSO_3^-$ anions in order to achieve a sensible refinement.

*Co-crystals of **HHTP** with TEA·Cl*

The structure crystallises in the monoclinic space group $P2_1/n$. One disordered diethyl ether molecule is present, as well as a further region of electron density, which appears to correspond to a partial occupancy diethyl ether molecule disordered about a special position. It was not possible to model this sensibly despite several attempts, and so PLATON-SQUEEZE[S14] was used to include this electron density in the refinement. The TEA cation also exhibits positional disorder. It was necessary to add restraints to the bond lengths and angles, as well as the thermal and vibrational ellipsoid parameters of the TEA cation and diethyl ether solvate to achieve a sensible refinement.

*Co-crystals of **HHTP** with TBA·Br*

Co-crystals of **HHTP** and TBA·Br were obtained by diffusing diethyl ether vapour into a methanol or a mixed acetone/methanol solution containing a 1:1 stoichiometric mixture of the two components. Four separate datasets were collected, but in all cases the data appear to be modulated (see Fig. S11), and typically could not be solved.

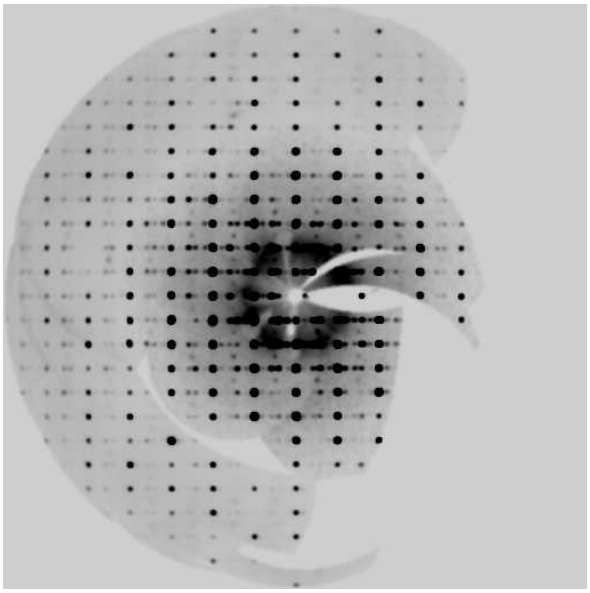

Fig. S11 Procession image (*h*,0,*l* plane) of co-crystals formed from **HHTP** and TBA·Br.

In one case, we were able to obtain a very crude solution, which is shown in Fig. S12. While this solution is of very poor quality, and could not be refined further, it appears to contain ten **HHTP** molecules, ten Br^- anions and a number of TBA cations (charge-balance arguments would suggest that there also ten cations, although they cannot all be identified with the very poor quality data). We tentatively assign this structure the formula [**HHTP**·TBA·Br]$_n$, and suggest that the high apparent Z' results from the modulation of the structure. This very crude solution seems to have the same overall structure as the rest of the structures reported in this paper (*i.e.* a 2D sheet formed of **HHTP** molecules and Br^- anions).

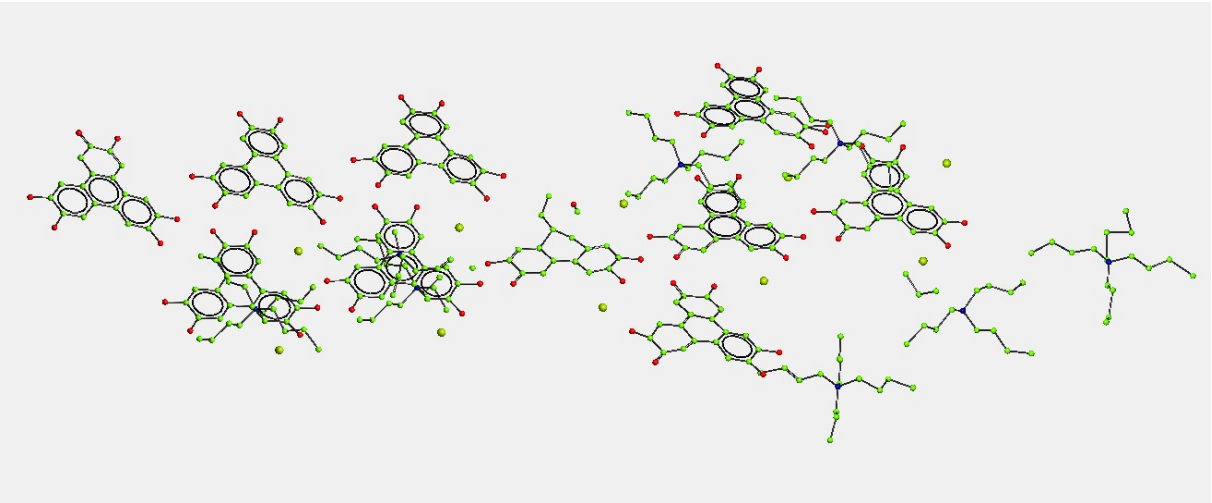

Fig. S12 Crude structure solution of co-crystals formed from **HHTP** and TBA·Br viewed in CRYSTALS.[S9] The results suggest a formula of [**HHTP**·TBA·Br]$_n$ consistent with the other structures in this paper.

Table S1. Selected crystallographic data for co-crystals of **HHTP** with tetraalkylammonium salts.

Compound	**HHTP·TBA·Cl**	**HHTP·TBA·I·*0.5H$_2$O***	**HHTP·TBA·H$_2$PO$_4$·*CH$_3$OH***
Radiation type	Cu	Mo	Mo
Temperature (K)	150	150	150
Chemical formula	2($C_{18}H_{12}O_6$)·2($C_{16}H_{36}N$)·2Cl	2$C_{18}H_{12}O_6$·2$C_{16}H_{36}N$·2I·0.5H_2O	$C_{18}H_{12}O_6$·$C_{16}H_{36}N$·H_2PO_4·CH_4O
Formula weight	1204.42	1396.34	695.79
a (Å)	11.18176(15)	21.6122(5)	12.7893(3)
b (Å)	15.2528(2)	16.4917(3)	16.0254(4)
c (Å)	19.3375(3)	21.8385(5)	17.4075(4)
α (º)	90	90	90
β (º)	90.2091(12)	117.021(3)	93.462(2)
γ (º)	90	90	90
Unit cell volume (Å^3)	3298.05(4)	6934.05(16)	3561.22(8)
Crystal system	monoclinic	monoclinic	monoclinic
Space group	*Pc*	$P2_1/c$	$P2_1/n$
Z	2	4	4
Reflections (all)	42683	66151	42134
Reflections (unique)	11012	14072	7214
R_{int}	0.025	0.037	0.045
R_1 [$I > 2\sigma(I)$]	0.040	0.041	0.049
$wR_2(F^2)$ (all data)	0.107	0.090	0.122

Compound	**HHTP·TBA·OAc·*MeOH***	**HHTP·TBA·MeOSO$_3$**	**HHTP·TEA·Cl·*C$_4$H$_{10}$O*[a]**
Radiation type	Cu	Cu	Mo
Temperature (K)	150	150	150
Chemical formula	$C_{18}H_{12}O_6$·$C_{16}H_{36}N$·$C_2H_3O_2$·CH_4O	2($C_{18}H_{12}O_6$)·2($C_{16}H_{36}N$)·2(CH_3SO_4)	$C_{18}H_{12}O_6$·$C_8H_{20}N$·Cl·$C_4H_{10}O$[a]
Formula weight	657.84	1355.72	564.12
a (Å)	13.0411(2)	20.01455(17)	11.2980(2)
b (Å)	16.2078(3)	15.41266(17)	15.7065(4)
c (Å)	16.6185(2)	22.33180(14)	17.8505(4)
α (º)	90	90	90
β (º)	90.0656(14)	90.0507(7)	90.914(2)
γ (º)	90	90	90
Unit cell volume (Å^3)	3512.61(5)	6888.86(4)	3167.20(7)
Crystal system	monoclinic	monoclinic	monoclinic
Space group	$P2_1/n$	$P2_1/c$	$P2_1/n$
Z	4	4	4
Reflections (all)	67938	117494	41261
Reflections (unique)	6945	13631	8086
R_{int}	0.035	0.032	0.082
R_1 [$I > 2\sigma(I)$]	0.077	0.047	0.095
$wR_2(F^2)$ (all data)	0.218	0.129	0.231

[a] NB: PLATON-SQUEEZE used.

[HHTP·TBA·Cl]$_n$

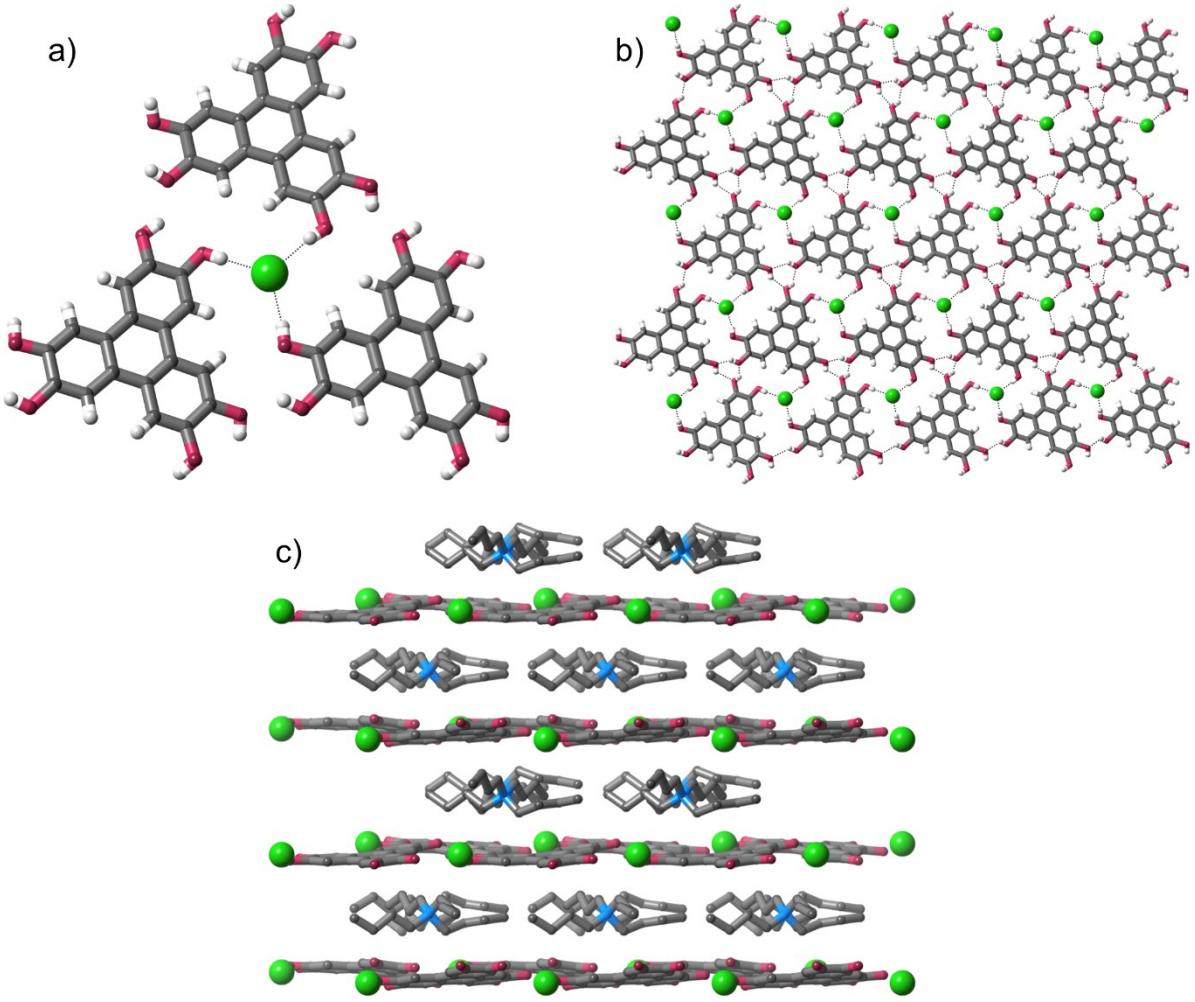

Fig. S13 Views of the solid state structure of [**HHTP**·TBA·Cl]$_n$: a) environment around Cl^- anion; b) 2D sheet formed from **HHTP** molecules and anions; c) packing viewed along *c* axis (with hydrogen atoms omitted for clarity). TBA cation disorder is omitted for clarity. *Please note that this is the same Figure as Fig. 1 in the manuscript, but is provided to allow easy comparison with Figs. S14–S18.*

[HHTP·TBA·I]$_n$

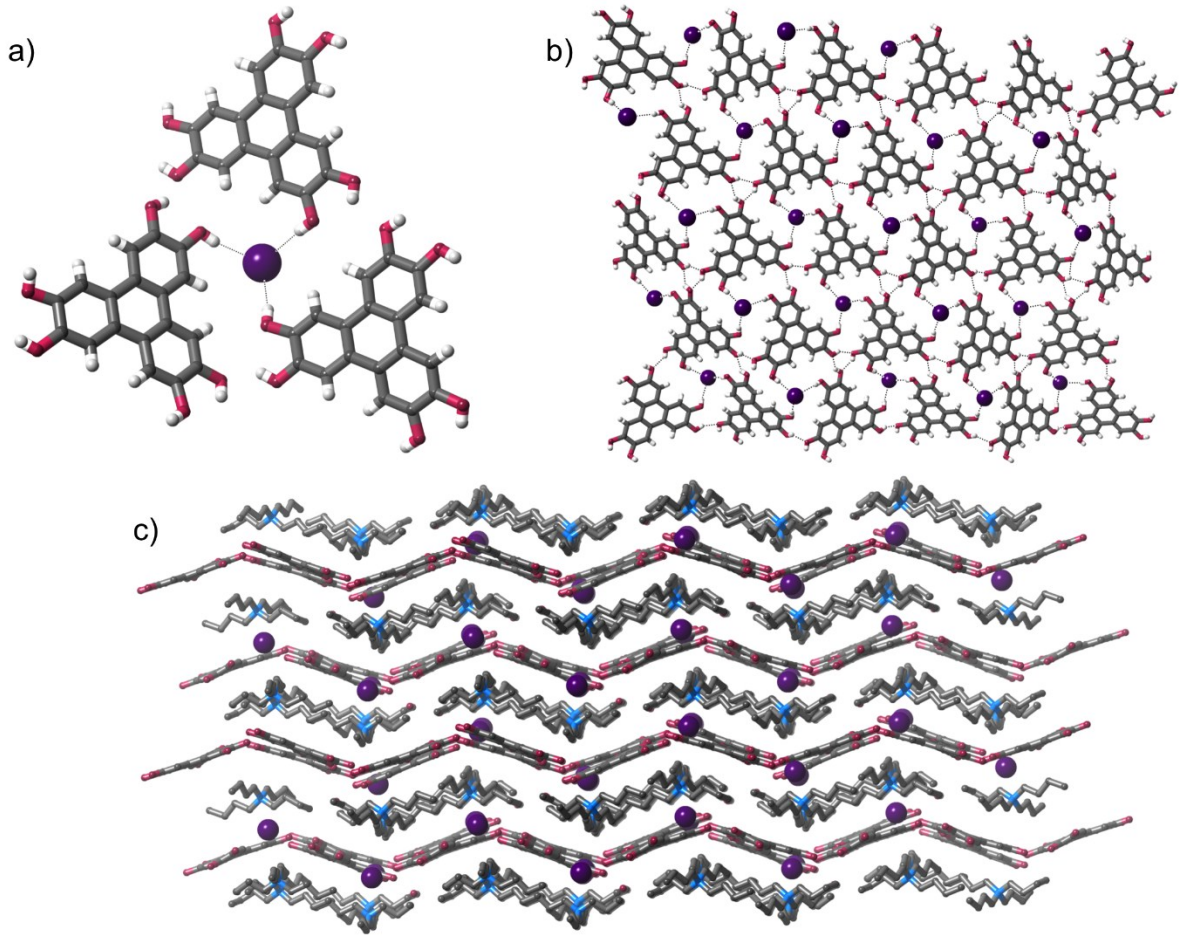

Fig. S14 Views of the solid state structure of [**HHTP**·TBA·I]$_n$: a) environment around I^- anion; b) 2D sheet formed from **HHTP** molecules and anions; c) packing (with hydrogen atoms omitted for clarity). TBA cation disorder is omitted for clarity.

[HHTP·TBA·H_2PO_4]$_n$

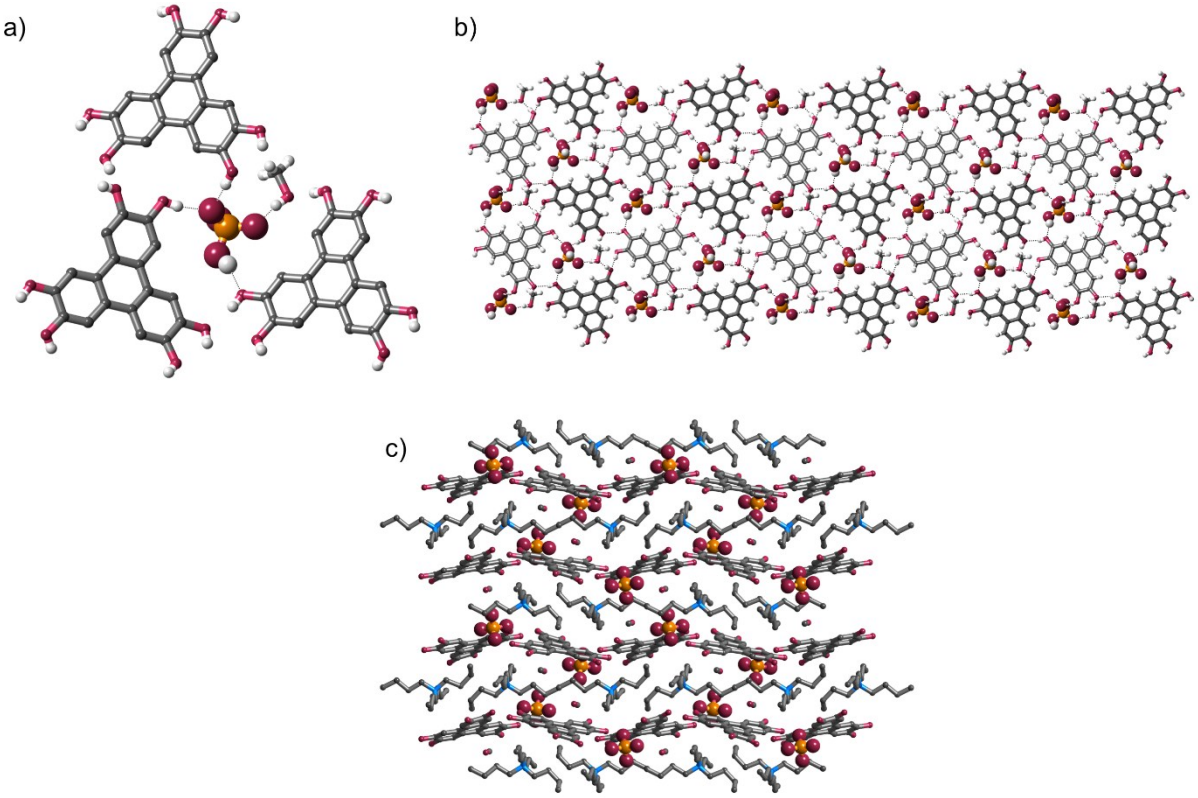

Fig. S15 Views of the solid state structure of [**HHTP**·TBA·H_2PO_4]$_n$: a) environment around $H_2PO_4^-$ anion; b) 2D sheet formed from **HHTP** molecules, anions and solvent; c) packing viewed along *a* axis (with hydrogen atoms omitted for clarity). TBA cation disorder is omitted for clarity.

[HHTP·TBA·OAc]$_n$

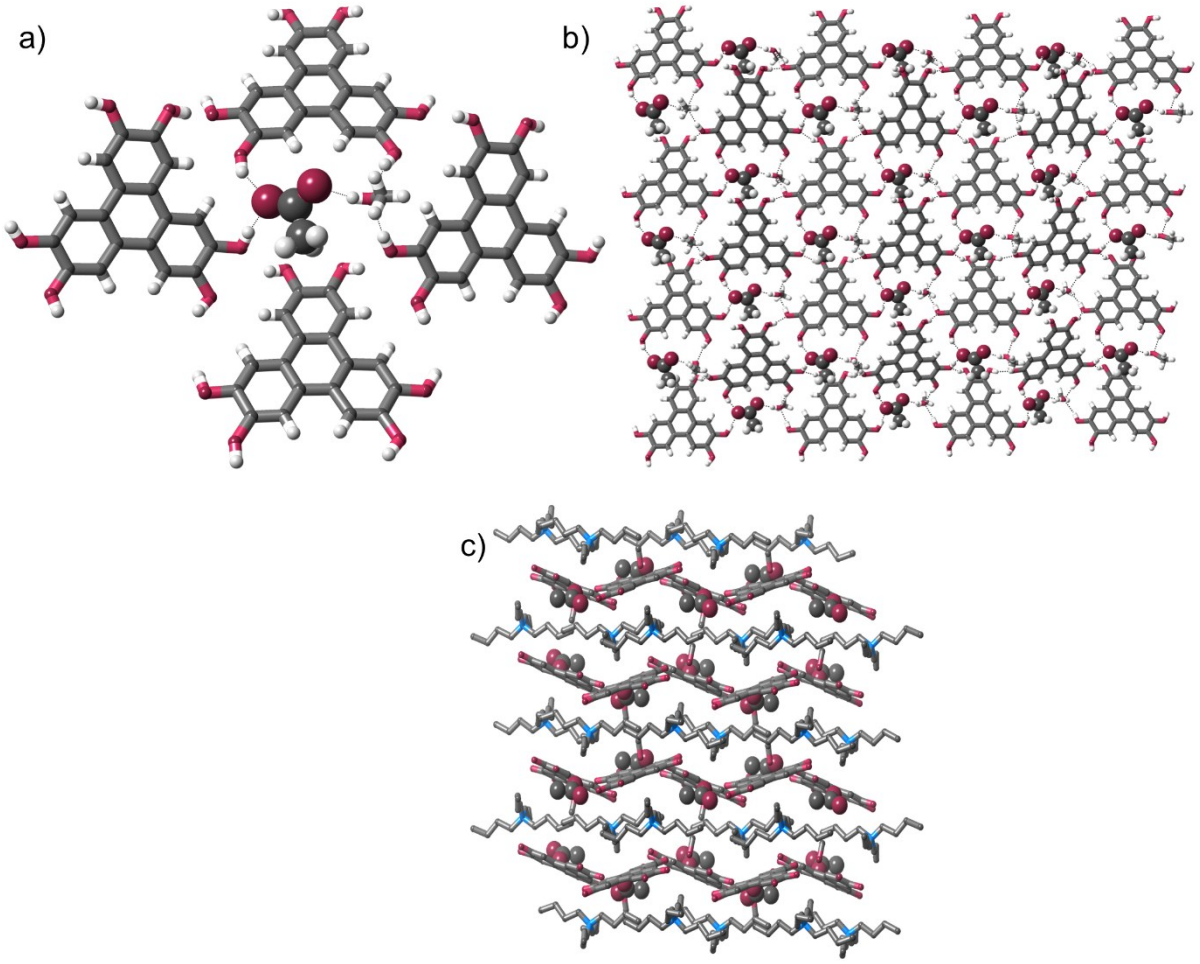

Fig. S16 Views of the solid state structure of [**HHTP**·TBA·OAc]$_n$: a) environment around OAc^- anion; b) 2D sheet formed from **HHTP** molecules, anions and solvent; c) packing viewed along *c* axis (with hydrogen atoms omitted for clarity). TBA cation disorder is omitted for clarity.

[HHTP·TBA·MeOSO$_3$]$_n$

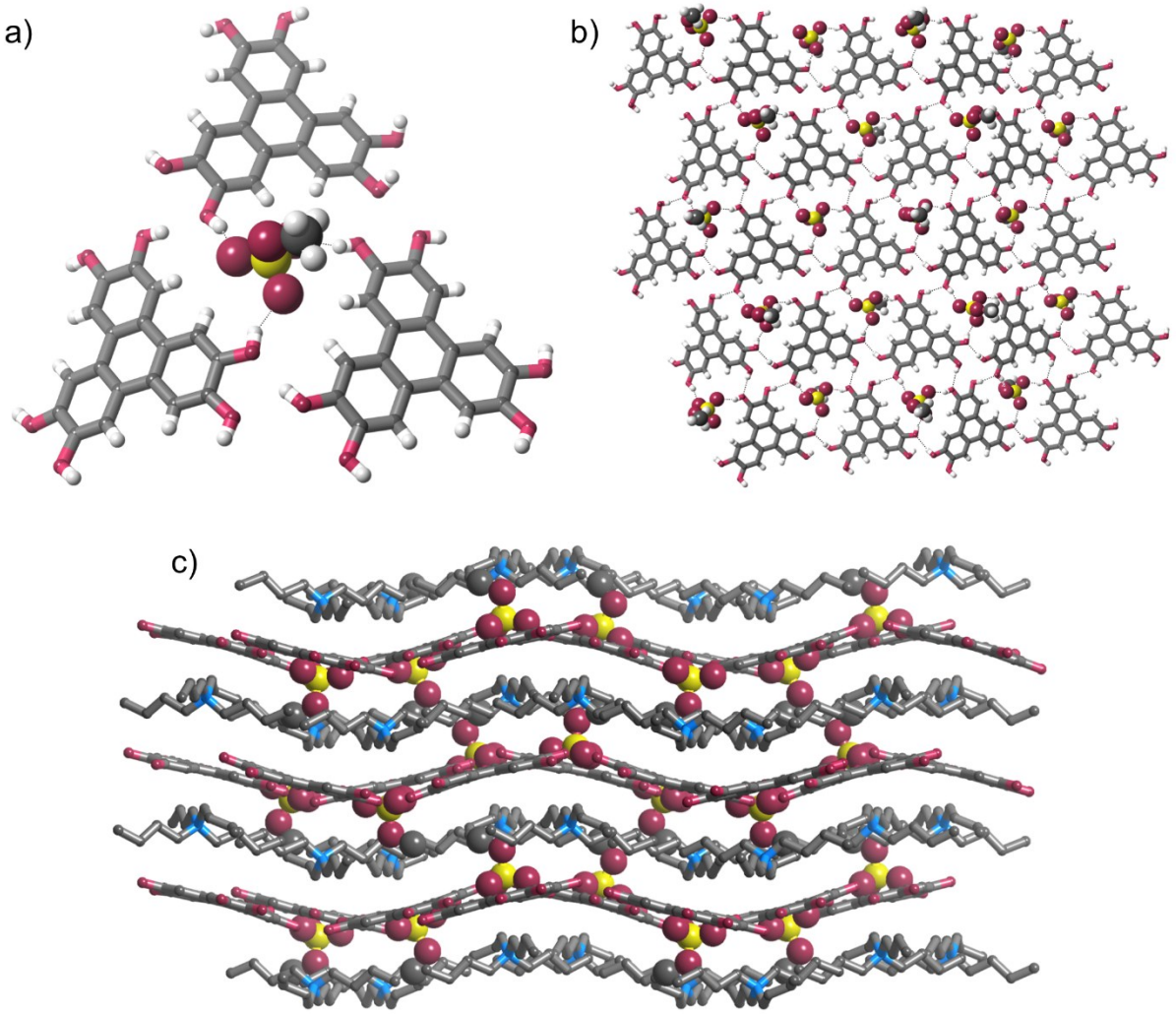

Fig. S17 Views of the solid state structure of [**HHTP**·TBA·MeOSO$_3$]$_n$: a) environment around MeOSO$_3^-$ anion; b) 2D sheet formed from **HHTP** molecules and anions; c) packing viewed along *c* axis (with hydrogen atoms omitted for clarity). TBA cation disorder is omitted for clarity.

[HHTP·TEA·Cl]$_n$

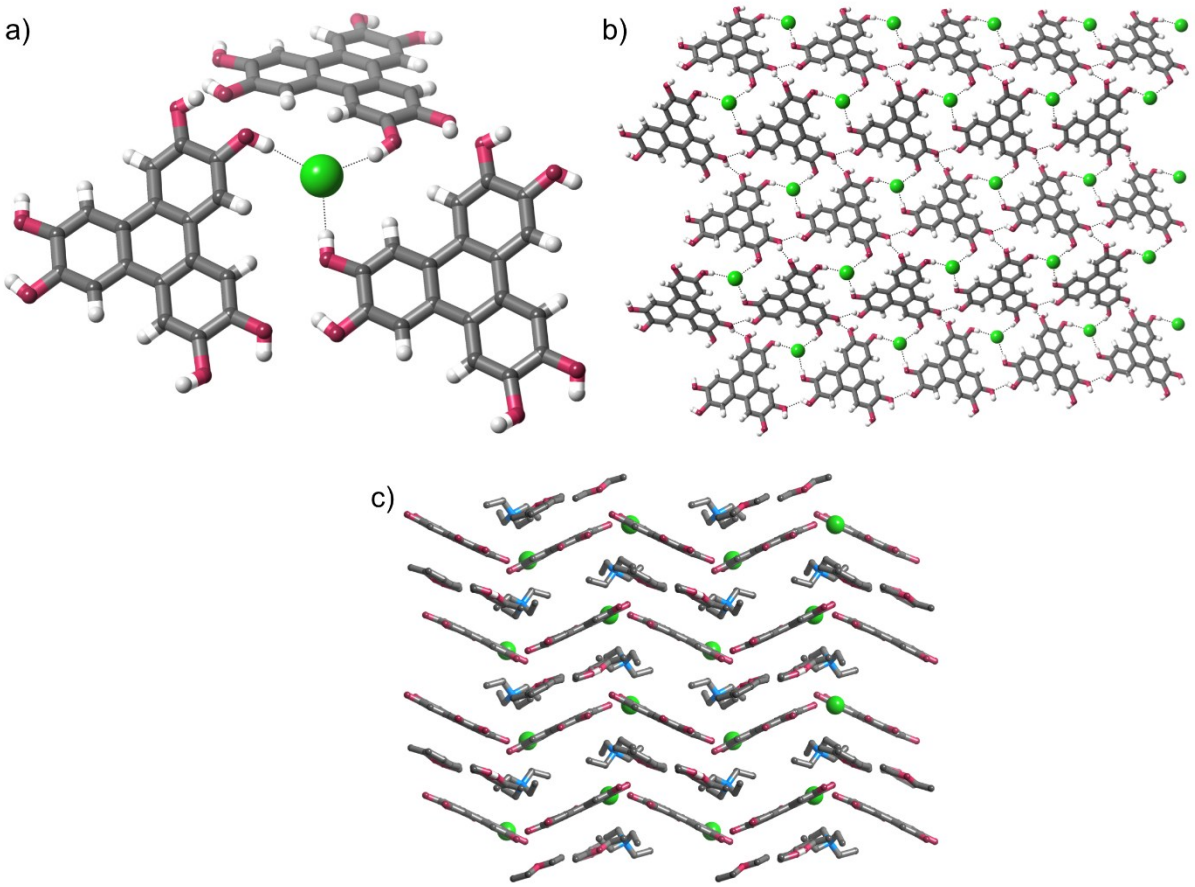

Fig. S18 Views of the solid state structure of [**HHTP**·TEA·Cl]$_n$: a) environment around Cl^- anion; b) 2D sheet formed from **HHTP** molecules and anions; c) packing viewed along *a* axis (with hydrogen atoms omitted for clarity). TEA cation and solvent disorder is omitted for clarity. NOTE: PLATON-SQUEEZE[S14] has been applied to this structure.

Details of PXRD experiments and PXRD traces

General comments

PXRD data were collected on the bulk materials for each of the anion-templated framework materials. Data were recorded at room temperature on a PANalytical Empyrean diffractometer using Cu Kα radiation and a PIXcel detector.

In order to usefully compare the SCXRD data (collected at 150 K) and PXRD data (collected at 293 K), basic Le Bail refinements of the PXRD data were performed in JANA2006,[S15] allowing the unit cell parameters to refine. These calculated 293 K unit cell parameters (Tables S2–S7) were then entered into the SCXRD CIF files and used to simulate an expected spectrum based on the SCXRD data (labelled "simulated" in Fig. 3 and Fig.s S19–S24), which is compared with the unrefined PXRD data. While this is clearly a reasonably crude way of accounting for the differences in temperature, and the refined unit cell parameters should be taken with caution, it allows a qualitative comparison between the PXRD and SCXRD data.

In all of the TBA-containing structures, the unit cell axes expand slightly on going from 150 K to 293 K as would be expected based on thermal expansion. In [**HHTP**·TEA·Cl]$_n$, the unit cell axes shrink. This is consistent with the observed major loss in crystallinity and collapse of the structure on drying.

[HHTP·TBA·Cl]$_n$

Table S2 Observed unit cell parameters for [**HHTP**·TBA·Cl]$_n$ determined by SCXRD and calculated unit cell parameters determined by Le Bail refinement of PXRD data.

Parameter	SCXRD data (150 K) Space group: *Pc*	Simulated from PXRD data (293 K)
a	11.18176(15)	11.2
b	15.2528(2)	15.6
c	19.3375(3)	19.4
α	90	90
β	90.2091(12)	90.6
γ	90	90

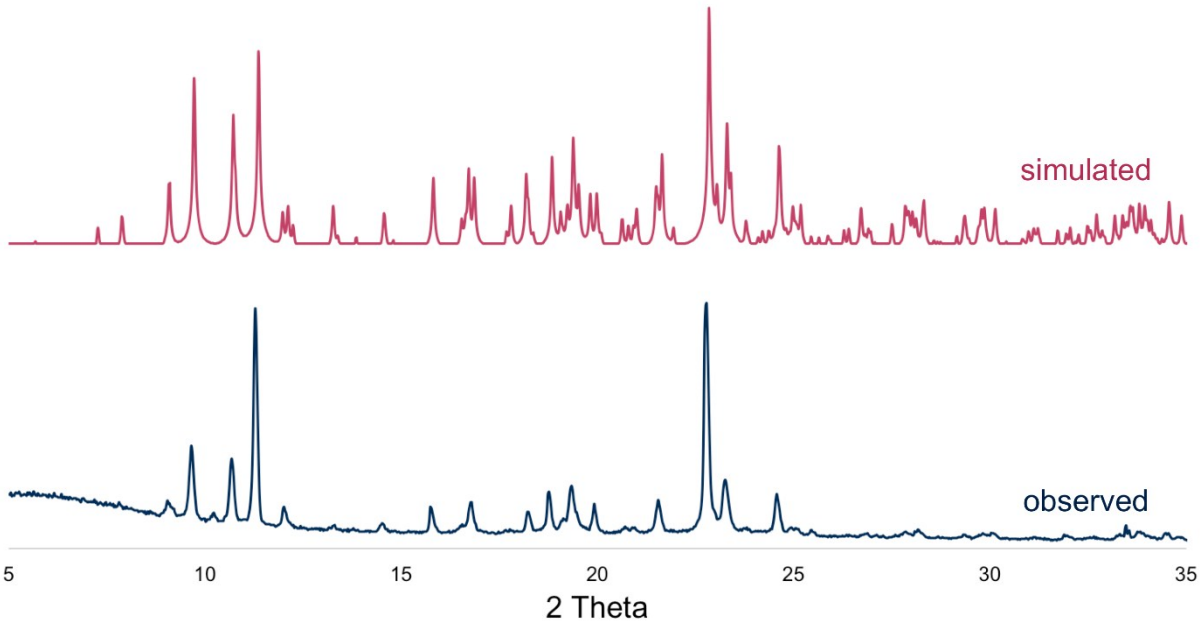

Fig. S19 PXRD trace and pattern simulated from SCXRD data for [**HHTP**·TBA·Cl]$_n$. *Please note that this is the same figure as Fig. 3a in the manuscript, but is provided to allow easy comparison with Figs. S20–S24.*

[HHTP·TBA·I]$_n$

Table S3 Observed unit cell parameters for [**HHTP**·TBA·I]$_n$ determined by SCXRD and calculated unit cell parameters determined by Le Bail refinement of PXRD data.

Parameter	SCXRD data (150 K) Space group: $P2_1/c$	Simulated from PXRD data (293 K)
a	21.6122(5)	21.9
b	16.4917(3)	17.1
c	21.8385(5)	22.1
α	90	90
β	117.021(3)	116.4
γ	90	90

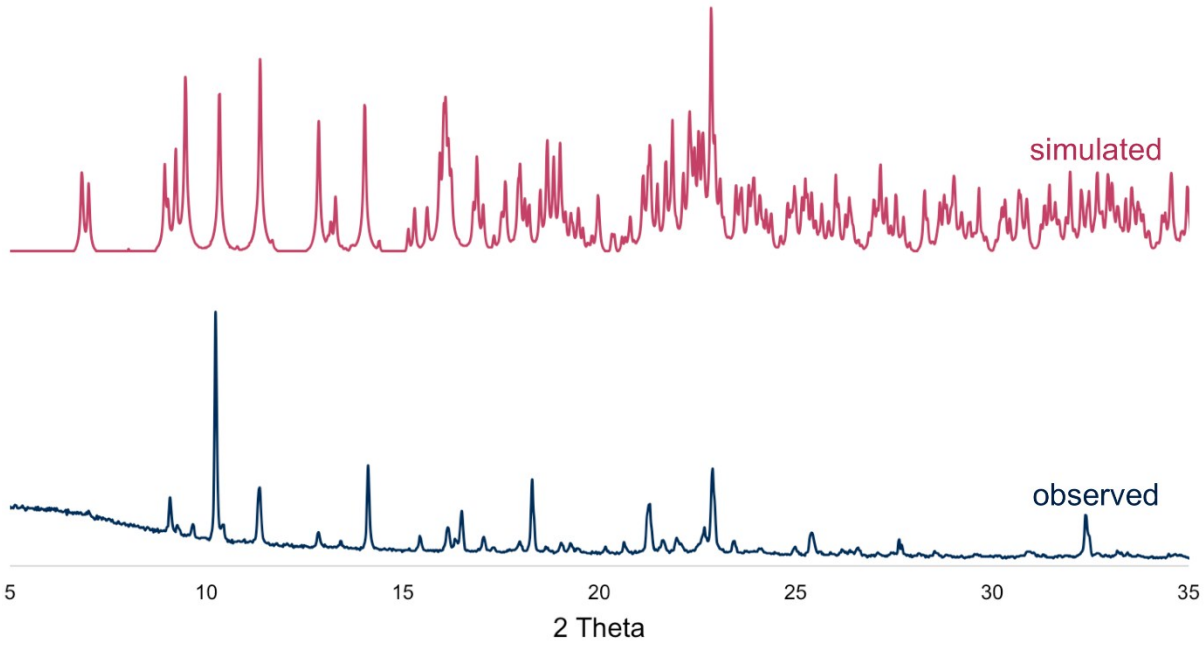

Fig. S20 PXRD trace and pattern simulated from SCXRD data for [**HHTP**·TBA·I]$_n$.

[HHTP·TBA·H_2PO_4]$_n$

Table S4 Observed unit cell parameters for [**HHTP**·TBA·H_2PO_4]$_n$ determined by SCXRD and calculated unit cell parameters determined by Le Bail refinement of PXRD data.

Parameter	SCXRD data (150 K) Space group: $P2_1/n$	Simulated from PXRD data (293 K)
a	12.7893(3)	12.9
b	16.0254(4)	16.2
c	17.4075(4)	17.5
α	90	90
β	93.462(2)	93.0
γ	90	90

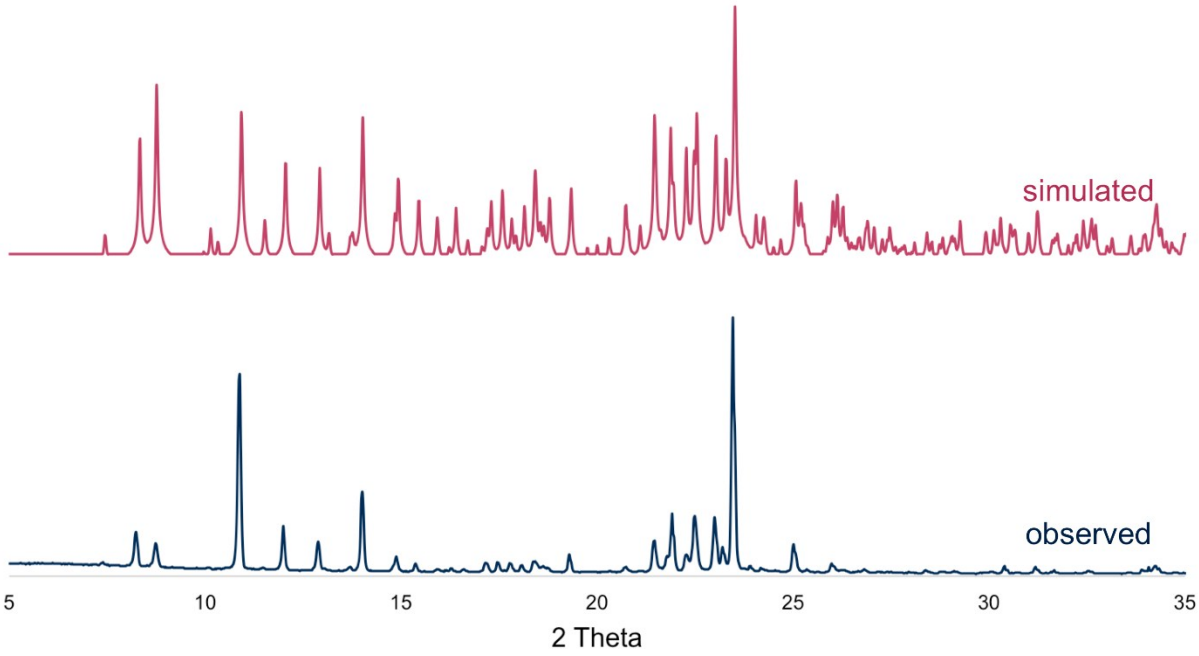

Fig. S21 PXRD trace and pattern simulated from SCXRD data for [**HHTP**·TBA·H_2PO_4]$_n$.

[HHTP·TBA·OAc]$_n$

Table S5 Observed unit cell parameters for [**HHTP**·TBA·OAc]$_n$ determined by SCXRD and calculated unit cell parameters determined by Le Bail refinement of PXRD data.

Parameter	SCXRD data (150 K) Space group: $P2_1/n$	Simulated from PXRD data (293 K)
a	13.0411(2)	13.0
b	16.2078(3)	16.5
c	16.6185(2)	16.6
α	90	90
β	90.0656(14)	90.7
γ	90	90

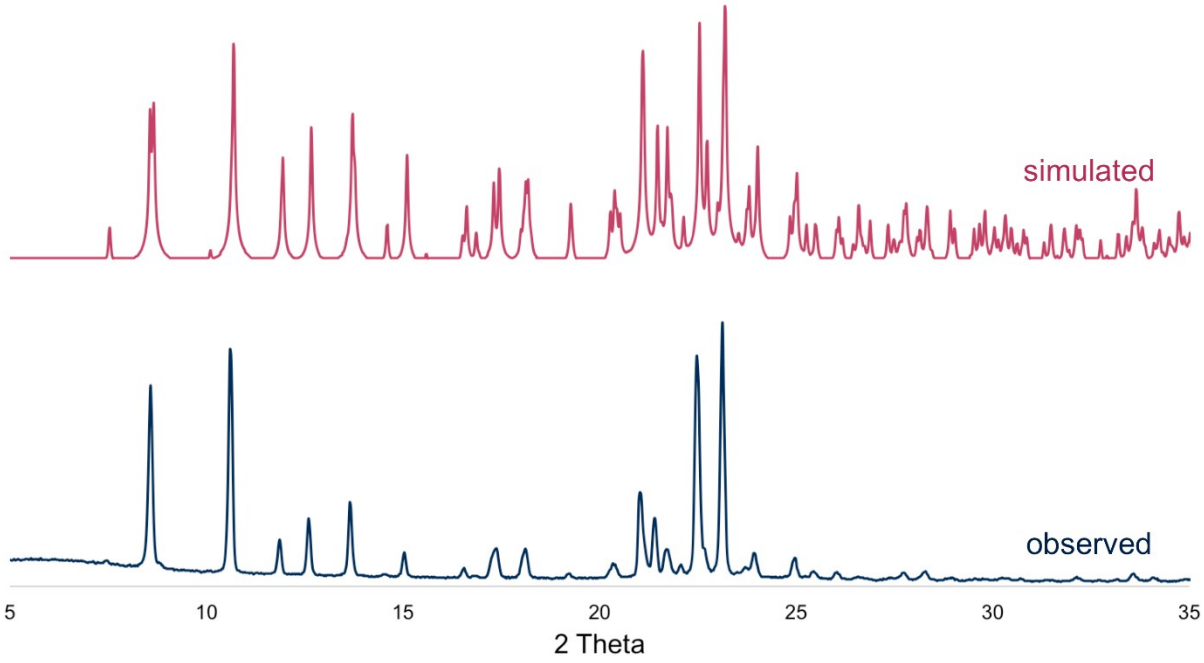

Fig. S22 PXRD trace and pattern simulated from SCXRD data for [**HHTP**·TBA·OAc]$_n$.

[HHTP·TBA·MeOSO$_3$]$_n$

Table S6 Observed unit cell parameters for [**HHTP**·TBA·0.5HSO$_4$·0.5MeOSO$_3$]$_n$ determined by SCXRD and calculated unit cell parameters determined by Le Bail refinement of PXRD data.

Parameter	SCXRD data (150 K) Space group: *P*2$_1$/*c*	Simulated from PXRD data (293 K)
a	20.01455(17)	20.0
b	15.41266(17)	15.7
c	22.33180(14)	22.4
α	90	90
β	90.0507(7)	90.7
γ	90	90

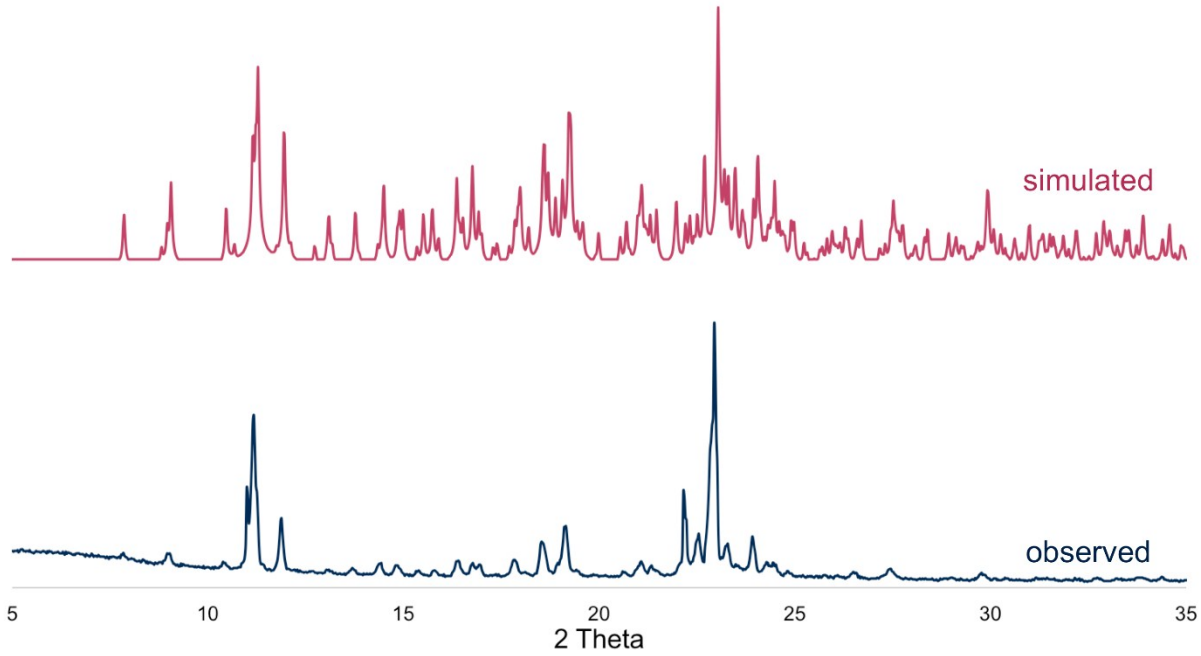

Fig. S23 PXRD trace and pattern simulated from SCXRD data for [**HHTP**·TBA·0.5HSO$_4$·0.5MeOSO$_3$]$_n$.

[HHTP·TEA·Cl]$_n$

Table S7 Observed unit cell parameters for [**HHTP**·TEA·Cl]$_n$ determined by SCXRD and calculated unit cell parameters determined by Le Bail refinement of PXRD data.

Parameter	SCXRD data (150 K) Space group: $P2_1/n$	Simulated from PXRD data (293 K)
a	11.2980(2)	11.0
b	15.7065(4)	15.2
c	17.8505(4)	17.4
α	90	90
β	90.914(2)	92.3
γ	90	90

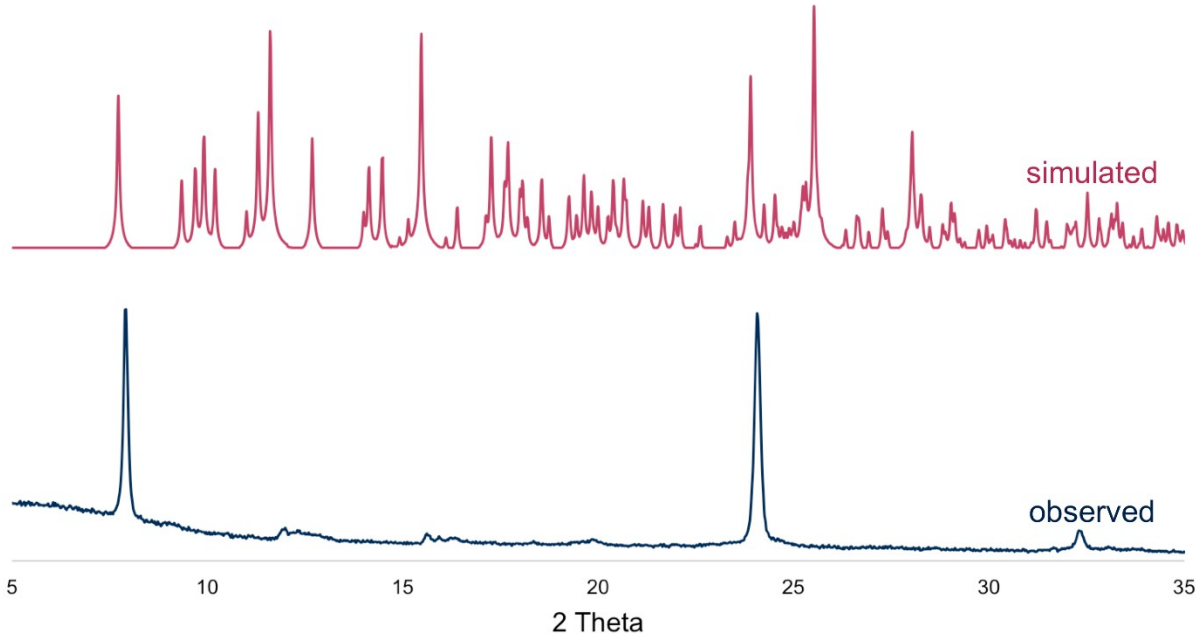

Fig. S24 PXRD trace and pattern simulated from SCXRD data for [**HHTP**·TEA·Cl]$_n$. *Please note that this is the same figure as Fig. 3b in the manuscript, but is provided to allow easy comparison with Figs. S19–S23.*

Thermogravimetric analysis

As can be seen in Fig. S25, the framework materials generally show relatively high thermal stability. In the halide anion containing systems, no significant weight loss (< 3%) is observed until 250 °C, at which point thermal decomposition begins.

In the case of the material containing HSO_4/$MeOSO_3$ anions, a weight loss of approximately 5% is observed between 225 and 270 °C, followed by complete thermal decomposition. In the structures containing OAc or H_2PO_4 anions, more complex thermal decomposition behaviour is observed with weight losses of 4–5% at relatively low temperature, followed by multi-step decompositions. It is suggested that the low temperature weight losses may be due to the loss of water adsorbed inside the materials (no organic solvents remain in the materials as shown by ^{1}H NMR spectroscopy, Figs. S3–S8; 4–5 wt% corresponds to approximately 1.5 water molecule per framework unit).

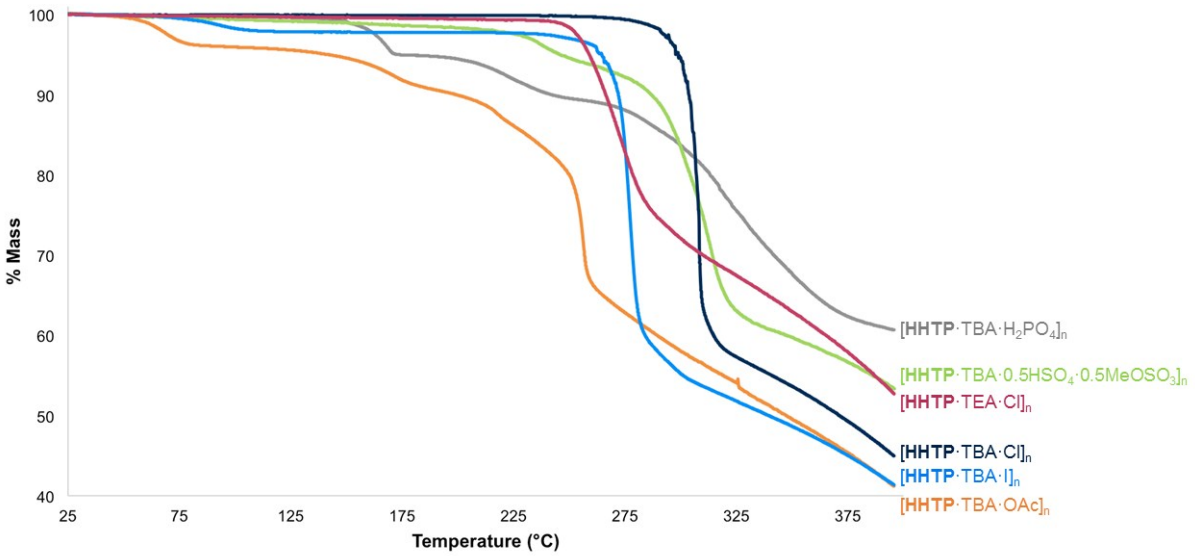

Fig.S25 Thermogravimetric analyses of framework materials prepared from **HHTP** (recorded at 10 °C/min under O_2).

References

[S1] H. E. Gottlieb, V. Kotlyar and A. Nudelman, *J. Org. Chem.*, 1997, **62**, 7512–7515.

[S2] D. Hao, J. Zhang, H. Lu, W. Leng, R. Ge, X. Dai and Y. Gao, *Chem. Commun.*, 2014**, 50**, 1462–1464.

[S3] K. Morimoto, T. Dohi and Y. Kita, *Eur. J. Org. Chem.*, 2013, 1659–1662.

[S4] E. Voisin and V. E. Williams, *Macromolecules*, 2008, **41**, 2994–2997.

[S5] F. Toda, K. Tanaka, T. Matsumoto, T. Nakai, I. Miyahara and K. Hirotsu, *J. Phys. Org. Chem.*, 2000, **13**, 39–45.

[S6] H. Naarmann, M. Hanack and R. Mattmer, *Synthesis*, 1994, 477–478.

[S7] J. Cosier and A. M. Glazer, *J. Appl. Crystallogr.*, 1986, **19**, 105–107.

[S8] Agilent Technologies, *CrysAlisPro*, 2011.

[S9] L. Palatinus and G. Chapuis, *J. Appl. Crystallogr.*, 2007, **40**, 786–790.

[S10] P. W. Betteridge, J. R. Carruthers, R. I. Cooper, K. Prout and D. J. Watkin, *J. Appl. Crystallogr.*, 2003, **36**, 1487.

[S11] R. I. Cooper, A. L Thompson and D. J. Watkin, *J. Appl. Crystallogr.*, 2010, **43**, 1017–1022.

[S12] R. Taylor and O. Kennard, *Acc. Chem. Res.*, 1984, **17**, 320–326.

[S13] R. I. Cooper, R. O. Gould, S. Parsons and D. J. Watkin, *J. Appl. Crystallogr.*, 2002, **35**, 168–174.

[S14] P. van der Sluis and A. L. Spek. *Acta Crystallogr.*, 1990, **A46**, 194–201; A. Spek, *J. Appl. Crystallogr.*, 2003, **36**, 7–13.

[S15] V. Petricek, M. Dusek and L. Palatinus, *Z. Kristallogr.*, 2014, **229**, 345-352.